

# Fingerprinting fractons with pump-probe spectroscopy

Wei-En Tseng, Oliver Hart, and Rahul Nandkishore  
Department of Physics and Center for Theory of Quantum Matter,  
University of Colorado Boulder, Boulder, Colorado 80309, USA  
(Dated: March 9, 2026)

We demonstrate how pump-probe techniques enable specific diagnostics of fracton phases of matter by exploring how lineon-planon braiding in the paradigmatic X-cube phase may be probed spectroscopically. Our discussion builds on works explaining how to probe anyonic exchange statistics spectroscopically in traditional spin liquids. However, the extension to fracton phases reveals qualitatively new features coming from the existence of multi-anyon bound states, which alter the long-time asymptotic behavior of the signal. In particular, the signal we examine is sensitive to (i) the existence of nontrivial braiding statistics in three dimensions, (ii) the fact that some of the fractionalized excitations can form bound states, and (iii) that some of the fractionalized excitations are lineonic in nature (i.e., mobile only in one dimension). Thus, one can spectroscopically detect not only the existence of anyonic braiding statistics in fracton phases, but can crisply distinguish it from anyons in traditional (non-fractonic) spin liquids.

*Introduction.*—Fracton phases of matter (see Refs. [1–3] for reviews) represent an exciting frontier for condensed matter physics. They connect to numerous research programs in theoretical physics, including constrained quantum dynamics, topological phases of matter, quantum error-correcting codes, and gravity. The connection most pertinent to the present work is the connection to topological phases. Now a key open question is: suppose a fracton phase were realized in some material – how could we diagnose it experimentally? We are particularly interested for the present work in *spectroscopic* diagnostics.

A partial answer was offered in Ref. [4], where it was pointed out that non-linear response (accessed through the technique of two-dimensional coherent spectroscopy [5]) could diagnose deconfinement (inherent in all topologically ordered phases, including fractons). However, it would be greatly desirable to have diagnostics tailored specifically for fractons. More recently, it was pointed out that nonlinear response has characteristic signatures of anyonic braiding statistics [6–8]. Since fracton phases also have nontrivial braiding relations for the excitations [9], it is tempting to ask whether these techniques could be applied to the fractonic context.

In this manuscript we demonstrate how ideas from Refs. [6–8] can be applied to the fractonic context, by probing *lineon-planon braiding* in the X-cube model [10], a paradigmatic example of a fracton phase. We further demonstrate that the fractonic realization of these ideas differs qualitatively from previous studies due to the existence of *planon bound states*, which have no analog in the original discussions [6–8]. The discussion in the main text is largely intuitive and phenomenological, with technical details relegated to the Appendices. The results demonstrate that the pump-probe nonlinear response signal is sensitive to (i) the existence of nontrivial braiding statistics in a three-dimensional system, (ii) to some of the fractionalized excitations forming bound states, and (iii) to some of the fractionalized excitations being mobile in only one dimension. This combination is highly suggestive of fractionalized excitations with subdimensional mobility,

a characteristic of fracton phases.

*X-cube model.*—Place qubits on the edges of a three-dimensional  $L \times L \times L$  cubic lattice. In the X-cube Hamiltonian [10, 11], qubits interact according to

$$H_{\text{XC}}(\mathbf{0}) = -J_x \sum_c A_c - J_z \sum_{v,\mu} B_v^\mu \quad (1)$$

where  $A_c$  is equal to the product of  $X_e$  for all  $e$  incident to the cube  $c$ , and  $B_v^\mu$  with  $\mu \in \{x, y, z\}$  is equal to the product of  $Z_e$  over the edges incident to vertex  $v$  in the plane perpendicular to  $\mu$ , i.e.,  $\{\partial e \ni v : e \perp \mu\}$ . We assume that the coupling constants  $J_x, J_z$  are positive.

The X-cube model has excitations with restricted mobility. Consider acting with a single  $Z_e$  operator on some edge  $e$ . This  $Z_e$  operator commutes with all  $B_v^\mu$  but anticommutes with the four  $A_c$  that contain the edge  $e$ . The four excited cubes  $A_c$  are called *fractons*, which are immobile when isolated. However, a pair of neighboring fractons, called a *planon*, is partially mobile under local operators. Suppose that  $e$  was oriented in the  $x$  direction, then pairs of defective  $A_c$  operators can be separated (with zero energy cost) by acting with a string of  $Z_e$  operators belonging to either the  $x$ - $y$  or  $z$ - $x$  planes. Such pairs of defective  $A_c$  operators are therefore mobile within a plane. We denote the excitation energy for a single planon as  $\Delta_p^0 = 4J_x$ .

The X-cube model also has *lineon* excitations. Consider acting with a single  $X_e$  operator on a  $z$ -oriented edge. This  $X_e$  operator commutes with all  $A_c$  operators but anticommutes with  $B_v^\mu$  such that  $v \in \partial e$  (the two vertices at the end of the edge  $e$ ) and  $\mu \perp z$ , corresponding to two neighboring lineons. The lineons can be separated (with zero energy cost) along the  $z$  axis by acting with  $X_e$  on neighboring  $z$ -oriented edges. Turning a corner requires creating additional lineons so lineon excitations reside at the endpoints of rigid 1D strings. We denote the excitation energy for a single lineon as  $\Delta_l^0 = 4J_z$ .

We now perturb the X-cube model by applying uniform magnetic fields in the  $x$  and  $z$  directions with strengths

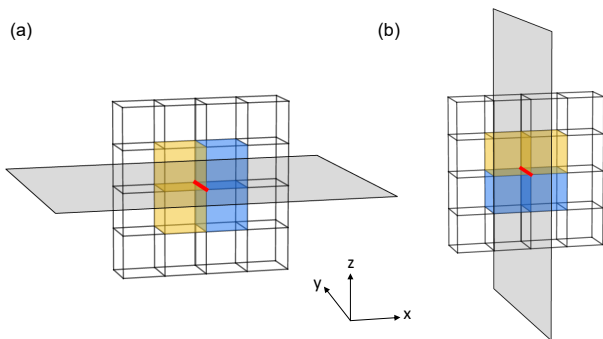


FIG. 1. Different pairings of four adjacent fractons with a single  $Z$  operator acting on a  $y$ -oriented link. (a) Planons separated in the  $x$ -direction can move in the  $xy$ -plane. This configuration is labeled by the relative coordinate as  $\mathbf{r}_{xy} = (1, 0)$ . (b) Planons separated in the  $z$ -direction can move in the  $yz$ -plane. This configuration is labeled as  $\mathbf{r}_{yz} = (0, 1)$ . (a) and (b) correspond to the same underlying wave function, thereby gluing together the  $xy$ - and  $yz$ -planes.

$h_x$  and  $h_z$ , respectively. The perturbed Hamiltonian is:

$$H_{\text{XC}}(\mathbf{h}) = H_{\text{XC}}(\mathbf{0}) - h_x \sum_e X_e - h_z \sum_e Z_e. \quad (2)$$

For  $h_x = h_z = 0$ , the excitations are eigenstates of  $H_{\text{XC}}$  and thus remain static. Turning on nonzero  $h_x$  and  $h_z$  leads to hybridization of the zero-field eigenstates and lineons and planons become dynamical. A state containing a pair of lineons is indexed by an unordered pair of vertices  $\{v_1, v_2\}$ . We denote the pair position by the center of mass  $\mathbf{R} = (v_1 + v_2)/2$  and the relative separation  $x = |v_2 - v_1|$  of the two lineons. A hardcore constraint is imposed at  $x = 0$ , since the two lineons cannot occupy the same site. For convenience, we take the system size to be infinite. The relative coordinate  $x \geq 1$  is then defined on a semi-infinite one-dimensional (1D) chain, while  $\mathbf{R}$  remains unconstrained. Using a Schrieffer–Wolff transformation, we obtain an effective 1D tight-binding Hamiltonian:

$$H_l = -h_x \sum_R \sum_{x \geq 1} |R \pm \frac{1}{2}, x \pm 1\rangle \langle R, x| \quad (3)$$

where  $|R \pm \frac{1}{2}, x \pm 1\rangle$  denotes the four states corresponding to each of the two lineons moving to the left and the right. Higher-order terms in  $h_x$  generate hopping processes over larger distances. The lineon-pair eigenstates are found by Fourier transformation:  $\langle R, x | \Psi_l \rangle = \Psi_l(R, x) = A e^{iK R} \sin kx$  with dispersion  $E_l(K, k) = -4h_x \cos(K/2) \cos k = -4h_x + \varepsilon_l(K, k)$ . Consequently, the energy gap to the two-lineon continuum is modified to  $2\Delta_l = 8J_z - 4h_x$ . The density of states (DOS) resembles that of a single-particle 2D tight-binding model (on a rectangular lattice) with a van Hove singularity (VHS) at half-filling  $E_l = 0$ . However, for a fixed  $K$ , the 1D DOS has a VHS at the band edges as  $g(\varepsilon_l) \sim 1/\sqrt{\varepsilon_l}$ . In a finite system,  $K$  and  $k$  are quantized according to the boundary conditions, as discussed in Appendix A.

*Planon bound state.*—For a pair of planons, we write the two-particle Hilbert space in terms of a center-of-mass coordinate  $\mathbf{R}$  and a difference coordinate  $\mathbf{r} = \mathbf{r}_1 - \mathbf{r}_2$  between the two planons. The identical nature of the two planons implies that we identify  $\mathbf{r}$  and  $-\mathbf{r}$ , so the planon-pair wavefunction factorizes as  $\Psi_p(\mathbf{R}, \mathbf{r}) = e^{i\mathbf{K} \cdot \mathbf{R}} \phi(\mathbf{r})$ , where  $\phi(\mathbf{r}) = \phi(-\mathbf{r})$ . Importantly, when four fractons sit on adjacent cube centers, they can be paired up into planons in different ways, as shown in Fig. 1. Consider the action of a single  $Z_e$  operator oriented along  $\hat{y}$ . This configuration can be viewed as a planon pair separated in the  $x$ -direction ( $\Delta x = 1$ ), which is allowed to move in the  $xy$  plane under the perturbed Hamiltonian  $H_{\text{XC}}(\mathbf{h})$ . We label this configuration by the difference coordinate  $\mathbf{r}_{xy} = (1, 0)$  in the  $xy$ -plane. Alternatively, the same four-fracton configuration can be regarded as a planon pair separated in the  $z$  direction ( $\Delta z = 1$ ), which is allowed to move in the  $yz$  plane, and we label it as  $\mathbf{r}_{yz} = (0, 1)$ . These two points describe exactly the same configuration, which glues the  $xy$  and  $yz$  planes together. The fact that planons can move in either the  $xy$  or  $yz$  planes, depending on how they are paired, means that they are not actually confined to move in a plane unless they are well separated. Nevertheless, one can still obtain an effective two-dimensional model by projecting out extra degrees of freedom. Focusing on the  $xy$ -plane by integrating out the  $yz$  plane, we expect to obtain an effective local potential at  $\mathbf{r}_{xy} = (1, 0)$ . Since we identify  $\mathbf{r}$  and  $-\mathbf{r}$ , the same local potential should also exist at  $\mathbf{r}_{xy} = (-1, 0)$ . Similarly, the action of a single  $Z_e$  operator oriented along  $\hat{x}$  creates a planon pair labeled by  $\mathbf{r}_{xy} = (0, 1)$  and  $\mathbf{r}_{xz} = (0, 1)$ , which glues the  $xy$ - and  $xz$ -plane. Projecting out the  $xz$ -plane results in local potentials at  $\mathbf{r}_{xy} = (0, \pm 1)$ . In addition, the two planons cannot reside on the same site, leading to a hardcore constraint at  $\mathbf{r}_{xy} = (0, 0)$ , modeled as an infinite on-site potential at the origin. Finally, the effective 2D tight-binding model for a planon pair can be expressed as:

$$H_p = -h_z \sum_{\mathbf{r}} \sum_{\delta = \pm \hat{x}, \pm \hat{y}} |\mathbf{R} + \delta/2, \mathbf{r} + \delta\rangle \langle \mathbf{R}, \mathbf{r}| + \sum_{\mathbf{r}} V(\mathbf{r}) |\mathbf{R}, \mathbf{r}\rangle \langle \mathbf{R}, \mathbf{r}|, \quad (4)$$

with

$$V(\mathbf{r}) = \begin{cases} \lambda \rightarrow \infty, & \mathbf{r} = (0, 0), \\ U(E), & \mathbf{r} = (\pm 1, 0); (0, \pm 1) \\ 0, & \text{otherwise.} \end{cases} \quad (5)$$

where we have written the relative coordinate as  $\mathbf{r} = \mathbf{r}_{xy}$ . In the absence of  $V(\mathbf{r})$ , the two-planon eigenenergies (expressed in terms of COM momentum  $\mathbf{K}$  and relative momentum  $\mathbf{k}$ ) are  $E(\mathbf{K}, \mathbf{k}) = -4h_z [\cos(K_x/2) \cos(k_x) + \cos(K_y/2) \cos(k_y)]$  which spans  $-8h_z \leq E \leq 8h_z$ . In the spatially uniformly excited case, we set  $\mathbf{K} = 0$ , and the bulk DOS has the same form as that of a 2D square lattice. Since  $V(\mathbf{r})$  is nonzero on only a finite set of sites, it does

not modify the bulk continuum DOS in the thermodynamic limit, although it does modify the scattering eigenstates. In addition, the energy-dependent local potentials are attractive  $U(E) < 0$  below the two-phonon continuum, which generate an additional phonon-pair bound state outside the continuum. Detailed analysis of the phonon's bound state and extended states are presented in Appendix B and C, respectively.

*Pump-probe response.*—The coexistence of bound and extended phonon states can provide a distinctive fingerprint of fracton order in pump-probe spectroscopy. We consider a pump pulse applied at time  $t = 0$  that creates a pair of lineons followed by a probe pulse at delay time  $t_1$  that creates a pair of phonons. The nonlinear pump-probe signal is extracted by subtracting the linear (unpumped) response,

$$L^3 \chi(t_1, t_2) = \langle A(t_1+t_2) A(t_1) \rangle_{\text{pump}} - \langle A(t_1+t_2) A(t_1) \rangle_0, \quad (6)$$

where  $A = \sum_e Z_e$  and  $L^3$  is a normalization volume. Here  $\langle \dots \rangle_0$  and  $\langle \dots \rangle_{\text{pump}}$  denote expectation values in the ground state and in the state prepared by the pump (containing a lineon pair), respectively. We consider that the only interaction between the phonons and the lineons is statistical with a phase factor  $(-1)^{n_l}$ , where  $n_l$  is the number of lineons (of the appropriate flavor) enclosed by the loop taken by the phonons [9]. The subtraction in Eq. 6 removes processes already present in linear response, so that only processes involving nontrivial braiding statistics between the pumped lineons and the probed phonons contribute to the nonlinear response. Microscopically, the statistical phase arises when the string operator of the lineon pair intersects the loop operator of the phonon pair. In the 3D X-cube model, the braiding processes occur when both the phonons and lineons are moving in the same plane, reducing it to a 2D problem. This can be seen by considering a lineon pair moving along  $\hat{x}$ , i.e. a string operator of  $X_e$  acts on the  $x$ -oriented links. If the phonon pair moves in the plane perpendicular to the lineon axis (the  $yz$ -plane), then the loop operators of  $Z_e$  only act on the  $y$ - and  $z$ -oriented links, and no nontrivial phase is generated because there are no intersections on the same link. As a result, braiding in the X-cube model can be thought of as decoupled 2D layers.

To quantify the braiding statistics, we follow the approach of Ref. [6]. The pumped lineons move in one dimension along semiclassical trajectories  $\mathbf{x}(t) = \pm \mathbf{v}t + \mathbf{x}_i$  with characteristic velocity  $\mathbf{v} = v\hat{x}$  and initial position  $\mathbf{x}_i$ . In a spacetime picture, the pumped lineon traces out a straight world-line, and the phonon pair with two trajectories  $\mathbf{r}_1(t)$  and  $\mathbf{r}_2(t)$  forms a closed loop between  $t_1$  and  $t_1+t_2$ . A topological phase is acquired only when the lineon world-line intersects the phonon's world-loop, as shown in Fig. 2. We denote the braiding probability as  $P[\mathbf{r}_{1,2}(t); v]$  for a given pair of phonon trajectories  $[\mathbf{r}_1(t), \mathbf{r}_2(t)]$  and lineon velocity  $v$ . The pump probe signal is then proportional to the linear response susceptibility and the braiding probability with additional weighting:  $\chi_{pp}(t_1, t_2) \propto \chi^{(1)}(t_2)[(-1)^{n_l} - 1]P[\mathbf{r}_{1,2}(t); v]$ . At long de-

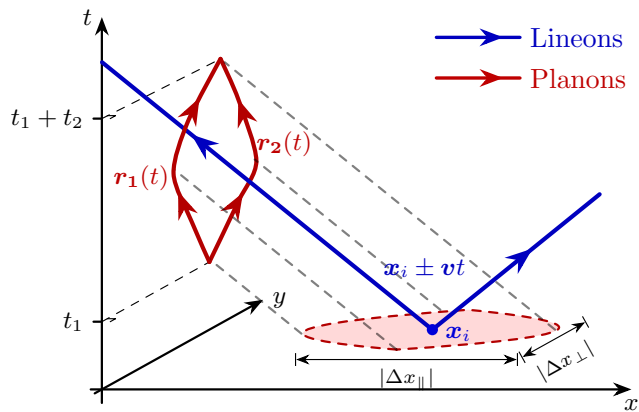


FIG. 2. Spacetime diagram of a pump-probe protocol for braiding statistics in the X-cube model. A pair of lineons is created at  $t = 0$ , which move in one dimension along the trajectories  $\mathbf{x} = \pm \mathbf{v}t + \mathbf{x}_i$ , where  $\mathbf{v} = v\hat{x}$ . A pair of phonons is created and annihilated at times  $t_1$  and  $t_1 + t_2$ , respectively, with trajectories labeled by  $\mathbf{r}_1(t)$  and  $\mathbf{r}_2(t)$  that together form a loop. The red shaded region indicates the two-dimensional area spanned by the initial lineon positions  $\mathbf{x}_i$  for which one of the lineon world-lines intersects the phonon world-loop. The braiding probability is therefore proportional to this area, which can be estimated as  $A[\mathbf{r}_{1,2}(t); v] \sim \Delta x_{\parallel} \Delta x_{\perp}$ , where  $\Delta x_{\parallel}$  and  $\Delta x_{\perp}$  denote the widths parallel and perpendicular to the lineon velocity.

lay times  $t_1$ , the two lineons created by the pump are typically far separated, so the subsequent probe phonon pair braids only one of them, and we set  $n_l = 1$ .

With the assumption of a homogeneous pump pulse, the initial position of the pump lineon  $\mathbf{x}_i$  is uniformly distributed in space. The braiding probability  $P[\mathbf{r}_{1,2}(t); v]$  can then be expressed in terms of an effective area  $A[\mathbf{r}_{1,2}(t); v]$  spanned by the initial lineon positions  $\mathbf{x}_i$ , within which the lineon world-line intersects the phonon world-loop. The time-dependence of the area can be estimated by separating the parallel width  $\Delta x_{\parallel}$  and the perpendicular width  $\Delta x_{\perp}$  to the lineon velocity  $\mathbf{v}$ . The perpendicular width is controlled by the typical separation of the two phonons in the direction perpendicular to the lineon,  $|\mathbf{r}_{1,\perp}(t) - \mathbf{r}_{2,\perp}(t)|$ . Due to the quantum broadening of the phonon's extended states, the perpendicular width scales as  $\Delta x_{\perp} \propto \sqrt{\hbar_z t_2}$  in both non-interacting and interacting cases, as shown in the Appendix D. In contrast, a bound pair of phonons does not spread in space, so  $\Delta x_{\perp} \sim O(1)$  remains a constant. On the other hand, the parallel width is classical: a lineon sweeps a length  $|v|t_2$  along its axis between  $t_1$  and  $t_1 + t_2$ , and shifting  $x_{\parallel}$  is equivalent to shifting the intersection time between the lineon and the phonon loop. Thus,  $\Delta x_{\parallel}$  can be approximated as  $|v|t_2$ . We note the spreading of the extended phonon states, which scales as  $\sqrt{\hbar_z t_2}$ , is subleading compared to  $\Delta x_{\parallel}$ . Therefore,  $\Delta x_{\parallel} \sim |v|t_2 + O(\sqrt{\hbar_z t_2})$  for the phonon extended states. To leading order, the area of initial conditions that yield braiding scales as  $A[\mathbf{r}_{1,2}(t); v] \approx \Delta x_{\parallel} \Delta x_{\perp} \propto |v|t_2 \times \sqrt{t_2}$  for the extended

states and  $A[\mathbf{r}_{1,2}(t); v] \propto |v|t_2$  for the bound state. By combining the braiding probabilities with the linear response signal, the pump-probe signal scales as

$$\chi_{pp}(t_1, t_2) \propto (-2)\chi^{(1)}(t_2) \times P[\mathbf{r}_{1,2}(t); v] \quad (7)$$

$$\propto \begin{cases} \chi_e^{(1)}(t_2)|v|t_2^{3/2}, & \text{extended states} \\ \chi_b^{(1)}(t_2)|v|t_2, & \text{bound state.} \end{cases} \quad (8)$$

where we have decomposed the linear-response susceptibility into contributions from extended states,  $\chi_e^{(1)}(t_2)$ , and from the bound state,  $\chi_b^{(1)}(t_2)$ , since they have distinct time scaling.

The linear response can be calculated by the correlation function with respect to the ground state:

$$\langle A(t_1 + t_2)A(t_1) \rangle_0 = L^3 e^{-iE_g(t_1-t_2)} \langle 2|e^{-iHt_2}|2 \rangle \quad (9)$$

where  $|2\rangle$  is the normalized, translation-invariant superposition of neighboring planon pairs, and  $E_g$  is the ground-state energy. For translation-invariant perturbations, the evaluation of the correlation function reduces to a single-particle problem in the relative coordinate. The relevant matrix element evaluates to

$$\langle 2|e^{-iHt_2}|2 \rangle = \int dE \rho(E) e^{-iEt_2} |\langle E|2 \rangle|^2 + e^{-iE_b t_2} |\langle E_b|2 \rangle|^2 \quad (10)$$

where the energy  $E$  is measured relative to the unperturbed two-planon state. The first term describes the continuum of extended states with  $-8h_z \leq E \leq 8h_z$ , while the second term accounts for a bound state at energy  $E_b < -8h_z$ . For extended states in the absence of the hardcore constraint, the matrix element is approximately constant near the band edges,  $\langle E|2 \rangle \sim 1/L$ , and the total density of states is also a constant and is extensive. The late-time asymptotics of the correlation function will be dominated by the band edges at  $E \approx \pm 8|h_z|$ , giving rise to  $\chi_e^{(1)}(t_2) \propto \sin(8h_z t_2)/t_2$  (see Appendix C for derivation). The  $1/t_2$  decay arises from the destructive interference of the continuum states, while the oscillations stem from the finite bandwidth of the lattice dispersion. When the hardcore constraint is included, the matrix element  $\langle E|2 \rangle$  becomes energy-dependent at the band edges, which in turn modifies the late-time dynamics. In Appendix C, we show that the interaction leads to multiplicative polylogarithmic corrections to the linear response, viz.

$$\chi_e^{(1)}(t_2) \propto \frac{\sin(8h_z t_2)}{t_2 \log(t_2)^2}. \quad (11)$$

On the other hand, the bound state does not overlap with the continuum, so its return probability does not decay, and  $\chi_b^{(1)}(t_2) \sim \text{const.} \times e^{iE_b t}$ . Combining these results with Eq. 8, we obtain:

$$|\chi_{pp}(t_1, t_2)| \propto \begin{cases} \sqrt{t_2}/\log(t_2)^2, & \text{extended states} \\ t_2, & \text{bound state} \end{cases} \quad (12)$$

Observe that the late-time behavior is in fact dominated by the planon bound state.

We next discuss the effect of a realistic pump pulse on the braiding-induced nonlinear response. We consider a Gaussian pump pulse with duration  $\tau$  and frequency detuning  $\delta$  from the bottom of the two-lineon band (assuming  $h \gg \delta, \tau^{-1}$ ), which excites a distribution of lineon pairs whose characteristic velocity and excitation density depend on the pump parameters. While these details modify the overall magnitude of the pump-probe signal, they do not affect its long-time scaling with  $t_2$ . In Appendix E, we show that the pump-probe coefficient (at a fixed time  $t_2$ ) scales as  $\chi_{pp}(\tau, \delta) \propto \chi^{(1)}\tau^0\delta^0$  for  $\delta\tau \ll 1$  and  $\chi_{pp}(\tau, \delta) \propto \chi^{(1)}\tau\delta$  for  $\delta\tau \gg 1$ , where  $\chi^{(1)}$  is the linear-response susceptibility of the planons. We note that although the lineon density of states exhibits a van Hove singularity near the band edge, this singularity is regularized even at the level of linear response by the vanishing excitation matrix element. Nevertheless, the independence of  $\chi_{pp}$  to  $\delta\tau$  in the limit  $\delta\tau \ll 1$  comes from the one-dimensional nature of the lineons. For braiding between two-dimensional particles,  $\chi_{pp} \propto \sqrt{\tau}$  in the limit  $\delta\tau \ll 1$  [6] (whereas for fully three-dimensional point particles there is no braiding). Thus, the  $\delta\tau \rightarrow 0$  limit of  $\chi_{pp}$  itself contains a signature of lineons. Finally, tuning the direction of the static magnetic field provides additional signatures for both linear and nonlinear responses (see Appendix F for further details), including regimes in which the nonlinear signal is suppressed or exhibits crossover behavior in time.

We have so far worked within a perturbative framework in which braiding events involve a single lineon. In this picture, the nonlinear signal increases with time indefinitely, implying an eventual breakdown of the perturbative expansion. This occurs because higher-order processes generate lineon multiplets, and braiding events involving multiple lineons (with even numbers giving a trivial phase) suppress the net statistical contribution, leading to a slowdown of the nonlinear signal. The time scale of the perturbative breakdown can be estimated as follows. Given a density of excited lineons  $\rho$  and the effective braiding area  $A[\mathbf{r}_{1,2}(t); v]$  computed before, we require the expected number of braided lineons to satisfy  $\langle n_l \rangle = \rho A[\mathbf{r}_{1,2}(t); v] \ll 1$ . Consequently, for sufficiently low excitation density, there exists a long time window in which the perturbative regime is valid and the increasing pump-probe signal due to statistical interactions can be observed. Moreover, since the effective braiding area of the planon's bound state grows as  $A[\mathbf{r}_{1,2}(t); v] \propto t_2$ , which is slower than that of extended states  $A[\mathbf{r}_{1,2}(t); v] \propto t_2^{3/2}$ , the increasing bound-state contribution remains perturbative to parametrically longer times.

*Conclusion.*—We have demonstrated how the existence of nontrivial lineon-planon braiding statistics can be probed spectroscopically in the X-cube model. Our discussion builds on analogous treatments for spin liquids [6–8], but has important differences. In particular, the relevant pump probe signal has asymptotic behavior that differs

from Ref. [6–8], and which is dominated by *planon bound states*, which have no analog in traditional spin liquids. The resulting signal (i) demonstrates the existence of nontrivial braiding statistics between excitations in a three dimensional system, and (ii) is sensitive to the existence of a bound state between some of the excitations with nontrivial braiding statistics, and (iii) to some of the fractionalized excitations being mobile in only one dimension. The combination of these features is highly suggestive of fractionalized excitations with subdimensional mobility, as is characteristic of (type-I) fracton phases. The discussion illustrates how pump-probe techniques can be used to formulate highly specific diagnostics for fracton phases, and how these diagnostics can differ in fracton phases from how they work in more traditional spin liquids. An extension of these ideas to other fracton phases (beyond the paradigmatic example of X-cube) is a worthwhile problem that is left for future work.

**Acknowledgements:** We acknowledge helpful discussions with Evan Wickenden. This work was supported by the U.S. Department of Energy, Office of Science, Basic Energy Sciences under Award No. DE-SC0021346.

## Appendix A: Boundary conditions of lineons

We consider a pair of lineons in a finite-size system, where the separation between the two lineons satisfies  $1 \leq x \leq L - 1$ . For convenience, we will work with system sizes with  $L$  odd. Note that (i) if  $R$  is an integer  $x$  must be even, while if  $R$  is a half-odd-integer then  $x$  must be odd, and (ii) in order to correctly handle periodic boundary conditions we must identify the states  $|R, x\rangle \equiv |R + L/2, L - x\rangle$ . We therefore choose to work with states  $|R, x\rangle$  such that  $x < L/2$  (while  $R$  is unconstrained), all of which are independent.

Acting with (2) on the lineon-pair state  $|R, x\rangle$ , we have

$$H_{\text{XC}}(h_x, h_z) |R, x\rangle = -h_x [|R - \frac{1}{2}, x + 1\rangle + |R - \frac{1}{2}, x - 1\rangle + |R + \frac{1}{2}, x + 1\rangle + |R + \frac{1}{2}, x - 1\rangle] \quad (\text{A1})$$

in the bulk. The four states on the right correspond to each of the two lineons moving to the left and the right. Higher-order expressions in  $h_x, h_z$  lead to hopping over larger distances. When  $x = 1$ , this is modified to

$$H_{\text{XC}}(h_x, h_z) |R, x\rangle = -h_x [|R - \frac{1}{2}, x + 1\rangle - h_x |R + \frac{1}{2}, x + 1\rangle] \quad (\text{A2})$$

since the lineons cannot be separated by less than one lattice site. For  $L$  odd and  $x = \lfloor L/2 \rfloor$  we have

$$H_{\text{XC}}(h_x, h_z) |R, x\rangle = -h_x [|R - \frac{1}{2}, x - 1\rangle + |R + \frac{1}{2}, x - 1\rangle + |R + \frac{L}{2} + \frac{1}{2}, x\rangle + |R + \frac{L}{2} - \frac{1}{2}, x\rangle], \quad (\text{A3})$$

since we have chosen to work with states satisfying  $x < L/2$ . The eigenstates and energies are found by Fourier

transformation. In particular, let  $\langle R, x | \Psi \rangle = \Psi(R, x) = A e^{iKR} \sin kx$ . Then  $H |\Psi\rangle = E |\Psi\rangle$  with

$$E(K, k) = -4h_x \cos(K/2) \cos k = -4h_x + \varepsilon_l(K, k). \quad (\text{A4})$$

Therefore, the energy cost to create a pair of lineon excitations is modified to  $2\Delta_l = 8J_z - 4h_x$ . The wave vectors  $k$  and  $K$  are quantized according to the solutions of

$$\frac{\sin[k(\lfloor L/2 \rfloor - 1)]}{\sin[k\lfloor L/2 \rfloor]} = 2 \cos k - e^{iKL/2} \quad (\text{A5})$$

$$\implies k = \begin{cases} \frac{\pi(2n_+ + 1)}{L} & \text{if } e^{iKL/2} = 1 \\ \frac{2\pi n_-}{L} & \text{if } e^{iKL/2} = -1 \end{cases}, \quad (\text{A6})$$

and  $K = 2\pi m/L$ , respectively. Note that  $e^{iKL/2} \in \{1, -1\}$ . Linearly independent for  $m \in \{0, 1, \dots, L - 1\}$ ,  $n_+ \in \{0, 1, \dots, \lfloor L/2 \rfloor - 1\}$ ,  $n_- \in \{1, 2, \dots, \lfloor L/2 \rfloor\}$ , giving  $L\lfloor L/2 \rfloor = L(L - 1)/2$  states in total, as required. The normalization constant is  $A = 2/L$ . Note that this analysis accounts for both the identical nature of the lineons and the hardcore constraint  $x \geq 1$  *exactly* to first order in the magnetic field strength  $h_x$ .

## Appendix B: Planon bound state

A pair of planons under static magnetic field can be mapped to an effective 2D tight-binding model (Eq. 4). Focusing on the uniformly excited center-of-mass sector with quasimomentum  $\mathbf{K} = 0$ , the two-body Hamiltonian in Eq. 4 reduces to a single-particle problem for the relative coordinate  $\mathbf{r}$ :

$$H_p = -2h_z \sum_{\mathbf{r}} \sum_{\delta=\pm\hat{x}, \pm\hat{y}} |\mathbf{r} + \delta\rangle \langle \mathbf{r}| + \sum_{\mathbf{r}} V(\mathbf{r}) |\mathbf{r}\rangle \langle \mathbf{r}|, \quad (\text{B1})$$

Note that the effective hopping becomes  $2h_z$  since either planon can hop and thus changes the relative coordinate with the same amplitude. The band dispersion is  $E(\mathbf{k}) = -4h_z(\cos k_x + \cos k_y)$ . The local potentials are

$$V(\mathbf{r}) = \begin{cases} \lambda \rightarrow \infty, & \mathbf{r} = (0, 0), \\ U(E), & \mathbf{r} = (\pm 1, 0); (0, \pm 1) \\ 0, & \text{otherwise.} \end{cases} \quad (\text{B2})$$

where the energy dependent local potentials  $U(E)$  originate from projecting out the extra degrees of freedom. Below the two-planon continuum  $E < -8h_z$ , the potential is attractive with  $U(E) < 0$ . In the absence of the hardcore constraint, any arbitrarily weak attractive potential produces at least one bound state. However, the hardcore constraint acts as an infinite repulsive potential at the origin, which introduces a threshold  $|U| > U_c$  for the bound-state solution. In the following, we first derive the threshold  $U_c$  in the presence of hardcore potential, then we calculate the effective energy-dependent potential  $U(E)$  obtained by projecting out the extra degrees

of freedom, and show that  $|U(E)|_{\max} > U_c$  satisfies the bound-state criterion for  $E < -8h_z$ . This proves the existence of a planon bound state and allows us to calculate the bound state energy.

We first decompose the perturbation into a repulsive part  $V_1 = \lambda|0\rangle\langle 0|$  and an attractive part  $V_2 = U\sum_{\mathbf{r}_i}|\mathbf{r}_i\rangle\langle\mathbf{r}_i|$ . We begin by computing the Green function under the perturbation  $V_1$ . The Dyson equation reads

$$G = G^0 + G^0V_1G^0 + G^0V_1G^0V_1G^0 + \dots = G^0 + G^0V_1G. \quad (\text{B3})$$

where  $G^0$  is the Green function for the unperturbed system. In real space this gives  $G_{\mathbf{r},\mathbf{r}'} = G_{\mathbf{r},\mathbf{r}'}^0 + \lambda G_{\mathbf{r},\mathbf{0}}^0 G_{\mathbf{0},\mathbf{r}'}^0$ . Solving for  $G_{\mathbf{0},\mathbf{r}'}$  and taking  $\lambda \rightarrow \infty$ , we find:

$$\begin{aligned} G_{\mathbf{r},\mathbf{r}'}(E) &= G_{\mathbf{r},\mathbf{r}'}^0 + \lambda \frac{G_{\mathbf{r},\mathbf{0}}^0 G_{\mathbf{0},\mathbf{r}'}^0}{1 - \lambda G_{\mathbf{0},\mathbf{0}}^0} = G_{\mathbf{r},\mathbf{r}'}^0 - \frac{G_{\mathbf{r},\mathbf{0}}^0 G_{\mathbf{0},\mathbf{r}'}^0}{G_{\mathbf{0},\mathbf{0}}^0} \\ &= G_{\mathbf{r}-\mathbf{r}'}^0 - \frac{G_{\mathbf{r}}^0 G_{\mathbf{r}'}^0}{G_0^0} \end{aligned} \quad (\text{B4})$$

where in the last step we used translational invariance of the unperturbed system. This relation connects the Green function in the presence of the hardcore constraint to the Green function of the clean system.

We now introduce the attractive potential

$$V_2 = U \sum_{\mathbf{r}_i} |\mathbf{r}_i\rangle\langle\mathbf{r}_i| = UP \quad (\text{B5})$$

where  $U < 0$  and  $P$  is the projector onto the subspace spanned by  $|\mathbf{r}_i\rangle$  with  $\mathbf{r}_1 = (1, 0)$ ,  $\mathbf{r}_2 = (-1, 0)$ ,  $\mathbf{r}_3 = (0, 1)$ ,  $\mathbf{r}_4 = (0, -1)$ . The full Green function  $\tilde{G}$  becomes:

$$\tilde{G} = \frac{G}{1 - V_2 G}. \quad (\text{B6})$$

where  $G$  is the Green function with a hardcore constraint at the origin (with  $V_1$  perturbation). The Bound states correspond to poles of the full Green function, that is  $\det(1 - V_2 G) = 0$ . Dividing the Hilbert space into the subspace spanned by  $|\mathbf{r}_i\rangle$  with projector  $P$  ( $P^2 = P$ ) and its complement (with projector  $1 - P$ ), the matrix can be written in block form as:

$$1 - V_2 G = \begin{pmatrix} 1 - UPGP & -UPG(1 - P) \\ 0 & 1 \end{pmatrix}. \quad (\text{B7})$$

The bound state solutions becomes

$$\det(1 - V_2 G) = \det(1 - UPGP) \quad (\text{B8})$$

$$= \det(\delta_{ij} - UG_{\mathbf{r}_i,\mathbf{r}_j}(E)) \quad (\text{B9})$$

$$= 0 \quad (\text{B10})$$

where  $G_{\mathbf{r}_i,\mathbf{r}_j} = \langle\mathbf{r}_i|G|\mathbf{r}_j\rangle$ . Therefore, the bound state solutions can be evaluated entirely within the subspace formed by  $|\mathbf{r}_i\rangle$ . For simplicity we define  $A \equiv G_{\mathbf{r}_1,\mathbf{r}_1}$ ,

$B \equiv G_{\mathbf{r}_1,\mathbf{r}_2}$  and  $C \equiv G_{\mathbf{r}_1,\mathbf{r}_3}$ . Due to symmetry, the  $4 \times 4$  matrix in the subspace can be explicitly written as

$$1 - UPGP = 1 - U \begin{pmatrix} A & B & C & C \\ B & A & C & C \\ C & C & A & B \\ C & C & B & A \end{pmatrix}. \quad (\text{B11})$$

Next, we can change the basis by defining the  $s, p_x, p_y, d$  states as linear combinations of  $|\mathbf{r}_i\rangle$ :

$$|s\rangle = (1, 1, 1, 1)^T / 2 \quad (\text{B12})$$

$$|p_x\rangle = (1, -1, 0, 0)^T / \sqrt{2} \quad (\text{B13})$$

$$|p_y\rangle = (0, 0, 1, -1)^T / \sqrt{2} \quad (\text{B14})$$

$$|d\rangle = (1, 1, -1, -1)^T / 2 \quad (\text{B15})$$

Under the change of basis, the matrix is diagonalized as  $\text{diag}(1 - Ug_s, 1 - Ug_{p_x}, 1 - Ug_{p_y}, 1 - Ug_d)$  where  $g_\alpha = \langle\alpha|G(E)|\alpha\rangle$ . We note that only the  $s$  and  $d$ -wave bound states are allowed by symmetry ( $\mathbf{r} \rightarrow -\mathbf{r}$ ). Therefore, the bound state conditions (the poles of the Green function) become:

$$U = 1/g_s(E) \quad (\text{B16})$$

$$U = 1/g_d(E) \quad (\text{B17})$$

It can be shown that  $g_s(E) = A + B + 2C$  while  $g_d(E) = A + B - 2C$ . Using the relation between  $G$  and the unperturbed Green function  $G^0$  in equation B4, we obtain  $A = G_0^0 - (G_{(1,0)}^0)^2/G_0^0$ ,  $B = G_{(2,0)}^0 - (G_{(1,0)}^0)^2/G_0^0$  and  $C = G_{(1,1)}^0 - (G_{(1,0)}^0)^2/G_0^0$ . As a result,

$$g_s(E) = G_0^0 + G_{(2,0)}^0 + 2G_{(1,1)}^0 - 4(G_{(1,0)}^0)^2/G_0^0 \quad (\text{B18})$$

$$g_d(E) = G_0^0 + G_{(2,0)}^0 - 2G_{(1,1)}^0 \quad (\text{B19})$$

where

$$\begin{aligned} G_{\mathbf{r}}^0(E) &= \langle\mathbf{r}|\frac{1}{E + i0^+ - H_0}|\mathbf{0}\rangle \\ &= \frac{1}{(2\pi)^2} \int d^2\mathbf{k} \frac{e^{i\mathbf{k}\cdot\mathbf{r}}}{E + i0^+ - E(\mathbf{k})}. \end{aligned} \quad (\text{B20})$$

where  $E(\mathbf{k}) = -4h_z(\cos k_x + \cos k_y)$ . Below the continuum,  $E < -8h_z$ , the Green functions  $G_{\mathbf{r}}^0(E) < 0$  and  $g_\alpha(E) < 0$  are negative. The clean Green function  $G_{\mathbf{r}}^0(E)$  vanishes as  $E \rightarrow -\infty$ , decreases monotonically as  $E$  increases, and diverges to  $-\infty$  as  $E \rightarrow -8h_z^-$ . Thus, in the absence of the hardcore constraint, any small attractive potential with  $U < 0$  can satisfy the bound state condition. However, with the hardcore constraint,  $g_\alpha(E)$  no longer diverges at the band edge because the divergence of the positive and negative terms cancel. Instead, it approaches a finite value  $g_{\min}$  as  $E \rightarrow -8h_z^-$ , leading to a threshold for bound-state formation for channel  $\alpha$ :

$$|U| \geq |g_{\alpha,\min}|^{-1} \equiv U_c^{(\alpha)} \quad (\text{B21})$$

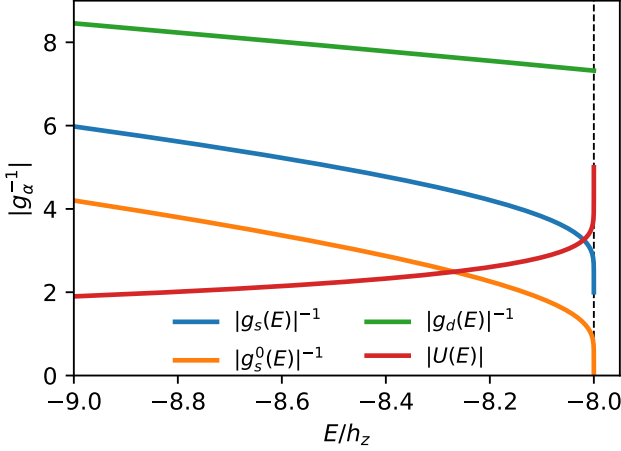


FIG. 3. The inverse Green's functions  $|g_s(E)|^{-1}$  and  $|g_d(E)|^{-1}$  denote the  $s$ - and  $d$ - wave channel in the presence of hardcore constraint, while  $|g_s^0(E)|^{-1}$  is the  $s$ -wave Green's function without the hardcore constraint. The edge of the two-phonon continuum locates at  $E/h_z = -8$ . The red curve shows the energy-dependent effective attractive potential  $|U(E)|$  obtained by integrating out the extra degrees of freedom. The bound state solution is given as  $|U(E)| = |g_\alpha(E)|^{-1}$ .

Numerical results for  $|g_s(E)|^{-1}$  and  $|g_d(E)|^{-1}$  are shown in Fig. 3 where  $|g_{s,\min}|^{-1} = 2h_z$  and  $|g_{d,\min}|^{-1} \approx 7.32h_z$  occurs at the band edge. For comparison, we also plot  $|g_s^0(E)|^{-1}$  where  $g_s^0(E) = G_{0,0}^0 + G_{2,0}^0 + 2G_{1,1}^0$  corresponds to the  $s$  wave channel in the absence of the hardcore constraint, which exhibits the expected divergence  $|g_s^0(E)|^{-1} \rightarrow 0$  at the band edge.

Our next step is to calculate the effective potential  $U(E)$  below the phonon continuum. The attractive potential arises from projecting out the extra degrees of freedom. In the two-dimensional description, the points  $\mathbf{r}_{xy} = (1, 0)$  and  $\mathbf{r}_{yz} = (0, 1)$  connect the  $xy$  and  $yz$  planes, but they represent the same state in the full Hilbert space. We must therefore remove this redundant degree of freedom. We choose to keep  $\mathbf{r}_{xy} = (1, 0)$  in  $H_{xy}$  while excluding the point  $\mathbf{r}_{yz} = (0, 1)$  from  $H_{yz}$ . From this perspective, excluding  $\mathbf{r}_{yz} = (0, 1)$  is equivalent to imposing an infinite repulsive potential at that site. As a result, the coupling between the two planes can be written as  $\tilde{V} = -2h_z \sum_{\mathbf{r}_i} |1, 0\rangle_{xy} \langle \mathbf{r}_i |_{yz}$  where  $|\mathbf{r}_i\rangle_{yz} = |1, 1\rangle, |-1, 1\rangle, |0, 2\rangle$  live in the  $yz$ -plane. The effective Hamiltonian obtained after integrating out the  $yz$ -plane is

$$\begin{aligned} H_{\text{eff}} &= H_{xy} + \tilde{V} \frac{1}{E - H_{yz}} \tilde{V}^\dagger \\ &= H_{xy} + 4h_z^2 \sum_{\mathbf{r}_i, \mathbf{r}_j} \langle \mathbf{r}_i | \frac{1}{E - H_{yz}} | \mathbf{r}_j \rangle |1, 0\rangle \langle 1, 0|_{xy} \\ &= H_{xy} + U(E) |1, 0\rangle \langle 1, 0|_{xy} \end{aligned} \quad (\text{B22})$$

Thus the effective on-site potential at  $\mathbf{r}_{xy} = (1, 0)$  is given by summing over the Green functions of the  $yz$ -plane with

the site  $\mathbf{r}_{yz} = (0, 1)$  removed. Shifting the coordinates in the  $yz$ -plane such that the infinite potential at  $\mathbf{r}_{yz} = (0, 1)$  now sits at the origin and using the relation in Eq. B4, we obtain:

$$\begin{aligned} U(E) &= 4h_z^2 \sum_{\mathbf{r}_i, \mathbf{r}_j} G_{\mathbf{r}_i, \mathbf{r}_j}(E) \quad (\text{B23}) \\ &= 4h_z^2 \left( 3G_0^0 + 4G_{(1,1)}^0 + 2G_{(2,0)}^0 - 9 \left( G_{(1,0)}^0 \right)^2 / G_0^0 \right) \\ &< 0 \end{aligned}$$

at location  $\mathbf{r}_{xy} = (1, 0)$ . Since we identify  $\mathbf{r}$  and  $-\mathbf{r}$ , the same local potential should also exist at  $\mathbf{r}_{xy} = (-1, 0)$ . Similarly, projecting out the  $xz$ -plane would lead to the same local potentials at  $\mathbf{r}_{xy} = (0, \pm 1)$ .

The magnitude of the local potential  $|U(E)|$  is energy dependent and increases monotonically as  $E$  approaches the band edge from below. In the limit  $E \rightarrow -8h_z^-$ , we find  $|U|_{\text{max}} = 5h_z$ . Comparing this with the thresholds obtained above, we observe that  $|U|_{\text{max}} > U_c^{(s)} = 2h_z$  for the  $s$ -wave channel, whereas  $|U|_{\text{max}} < U_c^{(d)} \approx 7.32h_z$  for the  $d$ -wave channel. Consequently, only a single  $s$ -wave phonon bound state appears in the energy gap. In Fig. 3, we plot  $|U(E)|$  along with  $|g_\alpha(E)|^{-1}$ , suggesting a  $s$ -wave bound state solution at a crossover as  $|U(E)| = |g_s(E)|^{-1}$ .

Inside the two-phonon continuum  $-8h_z \leq E \leq 8h_z$ , the effective local potential  $U(E)$  becomes complex. The real part is of order  $h_z$ , and changes sign between  $E < 0$  and  $E > 0$ . Recall that in the full interacting potential  $V(r)$ , the hardcore constraint at the origin has magnitude  $\lambda = 4J_x \gg h_z$ . As a result, the real part of  $U(E)$  on sites surrounding the origin can be viewed as a small renormalization of the effective hardcore strength and radius. In contrast, the imaginary part of  $U(E)$  encodes the non-Hermitian nature of the effective two-dimensional phonon-pair problem since the wavefunction can leak out to other 2D planes. Since the late-time dynamics is dominated by low energies, we focus on the unperturbed Green function near the bottom of the phonon band. Approximating the dispersion by  $E(k) \approx -8h_z + 2h_z k^2$ , the imaginary part of the unperturbed Green's function at energy  $E = -8h_z + \epsilon$  can be evaluated as

$$\begin{aligned} \text{Im} G_{\mathbf{r}}^0(E) &= \frac{1}{(2\pi)^2} \int d^2\mathbf{k} e^{i\mathbf{k}\cdot\mathbf{r}} [-\pi\delta(E - E(\mathbf{k}))] \\ &= -\frac{1}{4\pi} \int_0^\infty dk k \delta(\epsilon - 2h_z k^2) \int_0^{2\pi} d\theta e^{ikr \cos\theta} \\ &= -\frac{1}{8h_z} J_0 \left( \sqrt{\frac{\epsilon}{2h_z}} r \right) \\ &\approx -\frac{1}{8h_z} \left( 1 - \frac{\epsilon}{8h_z} r^2 \right) \end{aligned} \quad (\text{B24})$$

where  $J_0$  is the Bessel function of the first kind. As  $\epsilon \rightarrow 0^+$ ,  $\text{Im} G_{\mathbf{r}}^0(E)$  approach a constant  $-1/8h_z$ . In the same limit,  $\text{Im} U(E)$  in Eq. B23 vanishes, so the effective imaginary potential becomes relatively small near the band edge. Therefore, we conclude that  $\text{Im} U(E)$  has a negligible effect on the late-time dynamics of interest.

### Appendix C: Linear response for planons

We consider the effective Hamiltonian for the planon pair in Eq. B1 and impose open boundary conditions on the relative coordinate. Having ignored the interacting potential  $V(\mathbf{r})$ , the solutions are

$$C_{\mathbf{k}}(\mathbf{r}) = \frac{1}{N+1} \cos(k_x x) \cos(k_y y) \quad (\text{C1})$$

$$S_{\mathbf{k}}(\mathbf{r}) = \frac{1}{N+1} \sin(k_x x) \sin(k_y y), \quad (\text{C2})$$

which are symmetric under  $\mathbf{r} \rightarrow -\mathbf{r}$ . Here, the relative coordinate is defined on  $x, y \in [-N, N]$  where  $N = \lfloor L/2 \rfloor$ . In  $C_{\mathbf{k}}$ , the quasimomentum  $\mathbf{k}$  is quantized as  $k_\alpha = (n_\alpha + 1/2)\pi/(N+1)$  for  $n_\alpha \in \{0, 1, \dots, N\}$ . In  $S_{\mathbf{k}}$ , it is quantized as  $k_\alpha = n_\alpha \pi/(N+1)$  for  $n_\alpha \in \{1, \dots, N\}$ , giving  $2N^2 + 2N + 1$  states. This is consistent with the expected total number of states, equal to  $[(2N+1)^2 - 1]/2 + 1$ .

The quantity of interest is the return amplitude in Eq. 10. Here, we focus only on the extended states contribution where late times are dominated by the low-energy behavior of the overlap  $\langle E|2\rangle$  with the initial state  $|2\rangle = \frac{1}{2}(|(1, 0)\rangle + |(-1, 0)\rangle + |(0, 1)\rangle + |(0, -1)\rangle)$ . The overlap between  $|2\rangle$  and  $|C_{\mathbf{k}}\rangle$  is equal to  $(\cos k_x + \cos k_y)/(N+1) \approx 2/(N+1)$ , while its overlap with  $|S_{\mathbf{k}}\rangle$  vanishes. At low energies, the density of states is also independent of energy, behaving as  $\Theta(E)$  up to constants. Including only the states  $C_{\mathbf{k}}$ , the density of states that contribute to the late-time behavior is equal to  $(N+1)^2/8\pi h_z$ . Note that, on the lattice, we must also account for the high-energy states at  $E \approx 8|h_z|$  where the density of states is again constant near the top of the band. The late-time asymptotics of the correlation function will therefore be dominated by both band edges  $E \approx \pm 8h_z$ . We can then evaluate the late-time behavior of the return amplitude

$$I(t) = \int dE e^{-iEt} \rho(E) |\langle E|2\rangle|^2 \quad (\text{C3})$$

$$= \frac{i}{t} \left[ e^{-iEt} \rho(E) |\langle E|2\rangle|^2 \right]_{-8h_z}^{+8h_z} + O(t^{-2}) \quad (\text{C4})$$

$$\approx \frac{i}{2\pi h_z t} [e^{-i8h_z t} - e^{i8h_z t}] \quad (\text{C5})$$

$$= \frac{1}{\pi h_z t} \sin(8h_z t). \quad (\text{C6})$$

The linear response of extended states has a  $1/t$  decay envelope arising from the long-wavelength behavior, and oscillates at a frequency set by the lattice bandwidth since we work with a lattice model.

In the full interacting problem, there are additional effective local potentials surrounding the origin. For the band eigenenergies, the energy shifts induced by such local perturbation scale as  $O(1/L^2)$ . Consequently, the densities of states and the energy spectrum of the continuum remain unchanged in the thermodynamic limit. However, the eigenstates would acquire phase shifts due to the repulsive potential which acts as a scatterer. This

leads to an energy dependent of the overlap  $\langle E|2\rangle$  in low-energies. To make further analytical progress, we write lattice Laplacian in terms of a continuum derivative. This approximation is justified when the wavefunction varies smoothly on the lattice scale. The equation we would like to solve is

$$[-\nabla^2 + V_{\text{hc}}(r)]\psi(r, \theta) = \varepsilon_p \psi(r, \theta) \quad (\text{C7})$$

where  $V_{\text{hc}}(r)$  is taken to be infinite for  $r \leq b$  and zero otherwise, which encodes the hardcore constraint over a length scale  $b$ . The energy  $\varepsilon_p = E + 8h_z \approx 2h_z k^2$  is the energy relative to the bottom of the band. In cylindrical coordinates, this becomes

$$-\frac{\partial^2 \psi}{\partial r^2} - \frac{1}{r} \frac{\partial \psi}{\partial r} - \frac{1}{r^2} \frac{\partial^2 \psi}{\partial \theta^2} + V_{\text{hc}}(r)\psi = \varepsilon_p \psi \quad (\text{C8})$$

For simplicity, we modify the IR boundary conditions to be cylindrically symmetric. Namely we impose open boundary conditions,  $\psi(R, \theta) = 0$  at  $r = R$ . Since the problem now has cylindrical symmetry, angular momentum is a good quantum number and the general solution for the relative-coordinate wavefunction is  $\psi = e^{il\theta} \phi_l(r)$ , where  $\phi_l(r)$  satisfies the radial equation

$$-\frac{d^2 \phi_l}{dr^2} - \frac{1}{r} \frac{d\phi_l}{dr} + \frac{l^2}{r^2} \phi_l + V(r)\phi_l = \varepsilon_p \phi_l. \quad (\text{C9})$$

Since the planons are bosonic, the angular momentum quantum number  $l \in 2\mathbb{Z}$ , giving  $\psi(r, \theta) = \psi(r, \theta + \pi)$ . For  $r < b$ , we have  $\phi_l(r) = 0$  since  $V(r)$  is infinite. In the region  $r > b$ , the general solution to this equation is

$$\phi_l(r) = A_l J_{|l|}(kr) + B_l Y_{|l|}(kr) \quad (\text{C10})$$

where  $J_l$  and  $Y_l$  are Bessel functions of the first and second kind, respectively. We now implement the boundary conditions at  $r = b$  and  $r = R$ . The vanishing of the wave function at  $r = b$  requires that

$$\tan \delta_l = -B_l/A_l = J_{|l|}(kb)/Y_{|l|}(kb), \quad (\text{C11})$$

while the discreteness of the spectrum derives from the IR boundary condition,  $\phi_l(R) = 0$ . Up to normalization, the full solution (including COM coordinate  $\mathbf{R}$ ) is therefore

$$\Psi(\mathbf{R}, r, \theta) = C e^{i\mathbf{K} \cdot \mathbf{R}} e^{il\theta} [J_{|l|}(kr) - \tan \delta_l Y_{|l|}(kr)] \quad (\text{C12})$$

where  $\delta_l$  depends implicitly on the hardcore radius  $b$  and the relative momentum  $k$ . In the following, we set COM quasimomentum  $\mathbf{K} = 0$ .

In the interacting case, the late-time behavior is dominated by the  $l = 0$  channel. In this case,

$$\langle E|2\rangle = 2C_0(k) [J_0(k) - \tan \delta_0 Y_0(k)] \quad (\text{C13})$$

where  $C_0(k)$  is a normalization constant. Explicitly, the normalization constant is found by evaluating

$$\int_b^R 2\pi r dr [J_0(kr) - \tan \delta_0 Y_0(kr)]^2 = \pi (R^2 \varphi_{1,k}^2(kR) - b^2 \varphi_{1,k}^2(kb)) \quad (\text{C14})$$

where  $\varphi_{l,k}(kr) = J_{|l|}(kr) - \tan \delta_l(k) Y_{|l|}(kr)$  is the unnormalized wavefunction. Note that in Eq. (C14)  $k$  is implicitly determined by the quantization condition  $\varphi_{0,k}(kR) = 0$ . Thus,  $\varphi_{1,k}$  is being evaluated at  $k$  corresponding to  $l = 0$  and  $\varphi_{1,k}(kR)$  does *not* vanish. In the long-wavelength limit,  $kb \ll 1$ , we have  $\tan \delta_0 \sim (\log kb)^{-1} \ll 1$ . Note that system size  $R$  must be *very* large in order for  $\log b/R$  to be negligible. Nevertheless, in the remainder of this derivation we will assume that  $\log b/R \ll 1$ . In this case, the quantization condition is approximately  $J_0(kR) = 0$  and the allowed values of  $kR$  are determined by the Bessel function zeros  $j_{0,m}$  with the asymptotic expansion  $j_{l,m} = (m + l/2 - 1/4)\pi + O(1/(m + l/2))$ . Therefore, for  $R \gg b$  the normalization is approximately

$$\begin{aligned} & \int_b^R 2\pi r dr [J_0(kr) - \tan \delta_l Y_0(kr)]^2 \approx \pi R^2 J_1^2(kR) \\ & \approx \frac{2R}{k} + O[(k \log k)^{-1}] \end{aligned} \quad (\text{C15})$$

where we also assumed that  $kR \gg 1$ , equivalent to  $m \gg 1$  in the Bessel function zeros  $j_{0,m}$ . Hence, we obtain  $C_0(k) \approx \sqrt{k/2R}$ .

Near the bottom of the band, we can approximate  $\varepsilon_p = E + 8h_z \approx 2h_z k^2$ . In the long-wavelength regime  $k \ll 1$ , the Bessel functions can be approximated by

$$J_0(x) \approx 1, \quad Y_0(x) \approx \frac{2}{\pi} \left[ \log \frac{1}{2} x + \gamma \right]. \quad (\text{C16})$$

The logarithmic singularity of  $Y_0(x)$  at  $k = 0$  will dominate the late-time behavior. At low energies, the matrix element is approximated by

$$\begin{aligned} \langle E|2\rangle & \approx 2C_0(k) \left[ 1 - \frac{\log(k/2) + \gamma}{\log(bk/2) + \gamma} \right] \\ & = \frac{2C_0(k) \log b}{\log k + \log b/2 + \gamma} \\ & \approx \sqrt{\frac{2k \log b}{R \log k}} \end{aligned} \quad (\text{C17})$$

with an analogous expression at the top of the band near  $E \approx 8h_z$ . Next, we evaluate the low-energy density of states for the  $l = 0$  states  $\rho(E) = \frac{dN}{dk} \frac{dk}{dE} \approx \rho_0/(4h_z k)$  where  $\rho_0 \equiv dN/dk$  can be obtained by imposing the boundary condition:

$$J_0(kR) - \tan \delta_0 Y_0(kR) \stackrel{!}{=} 0. \quad (\text{C18})$$

At low energies, the arguments  $kR \sim 1$ , implying that  $kb \ll 1$ . Therefore  $Y_0(kR) \ll Y_0(kb)$  and the solutions are given approximately by the solutions of

$$J_0(kR) = 0, \quad (\text{C19})$$

whose density is  $\rho_0 = R/\pi$ . We therefore arrive at the

final result

$$\begin{aligned} I(t) & = \int dE e^{-iEt} \rho(E) |\langle E|2\rangle|^2 \\ & = \frac{2}{R} (\log b)^2 \rho_0 [e^{-8ih_z t} - e^{8ih_z t}] \frac{i}{h_z t \log(t)^2} \\ & = \frac{4(\log b)^2 \sin(8h_z t)}{\pi h_z t \log(t)^2}, \end{aligned} \quad (\text{C20})$$

This result shows that the interactions lead to polylog corrections in time to the noninteracting  $1/t$  decay.

#### Appendix D: Planon typical width

Now, we derive the typical separation of a planon pair that returns to the initial state  $|2\rangle$  after a time interval  $t_2$ . The typical separation sets the perpendicular width  $\Delta x_\perp$  in the pump-probe response. Recall that the return amplitude is

$$I(t_2) = \langle 2|e^{-iHt_2}|2\rangle = \sum_{\mathbf{r}} \langle 2|e^{-iH(t_2-\tau)}|\mathbf{r}\rangle \langle \mathbf{r}|e^{-iH\tau}|2\rangle \quad (\text{D1})$$

where we insert an intermediate time  $0 < \tau < t_2$ , at which the planon-pair state  $|\mathbf{r}\rangle$  is represented by the difference coordinate ( $\mathbf{r} = \mathbf{r}_1 - \mathbf{r}_2$ ). For simplicity, we first consider the free propagator in two dimensions:

$$\langle \mathbf{r}'|e^{-iHt}|\mathbf{r}\rangle = \frac{m}{2\pi i t} e^{i\frac{m|\mathbf{r}-\mathbf{r}'|^2}{2t}} \quad (\text{D2})$$

The initial state  $|2\rangle = \frac{1}{2}(|(1,0)\rangle + |(-1,0)\rangle + |(0,1)\rangle + |(0,-1)\rangle)$ . At late times and on length scales large compared with the lattice spacing ( $r \gg 1$ ), the free propagator from  $|2\rangle$  to  $|\mathbf{r}\rangle$  can be approximated as

$$\begin{aligned} \langle \mathbf{r}|e^{-iHt}|2\rangle & = \frac{m}{2\pi i t} e^{i\frac{m(|\mathbf{r}|^2+1)}{2t}} \left[ \cos \frac{mr_x}{t} + \cos \frac{mr_y}{t} \right] \\ & \approx \frac{m}{\pi i t} e^{i\frac{m|\mathbf{r}|^2}{2t}} \end{aligned} \quad (\text{D3})$$

where in the last step we used  $mr/t \ll 1$  at late times. It then follows that

$$I(t_2) = -\frac{m^2}{\pi^2} \frac{1}{\tau(t_2 - \tau)} \int d^2\mathbf{r} e^{i\alpha(t_2, \tau)|\mathbf{r}|^2} \quad (\text{D4})$$

where

$$\alpha(t_2, \tau) = \frac{m}{2} \left( \frac{1}{\tau} + \frac{1}{t_2 - \tau} \right) \quad (\text{D5})$$

In the 2D spatial integral, contributions from separations satisfying  $\alpha(t_2, \tau)|\mathbf{r}|^2 > 1$  oscillate rapidly and mostly cancel. Thus, the typical distance is set by  $|\mathbf{r}|_{\text{typ}}^2 \sim 1/\alpha(t_2, \tau)$ :

$$|\mathbf{r}|_{\text{typ}}^2 \sim \frac{2}{m} \frac{\tau(t_2 - \tau)}{t_2} \quad (\text{D6})$$

Near the bottom band edge, the planon's band dispersion can be approximated as  $\varepsilon_p \approx 2h_z k^2 \approx k^2/2m$  with the effective mass  $m = 1/4h_z$ . The maximum typical separation occurs at mid-time  $\tau = t_2/2$ , which yields

$$|\mathbf{r}|_{\max} = \sqrt{2h_z t_2} \quad (\text{D7})$$

As a result, the planon perpendicular width scales as  $\Delta x_{\perp} \sim \sqrt{h_z t_2}$  in the noninteracting case.

We now comment on the modification due to the hardcore constraint. The propagator can be written in the energy basis as

$$K(\mathbf{r}, t) = \langle \mathbf{r} | e^{-iHt} | 2 \rangle = \int dE \rho(E) \langle \mathbf{r} | E \rangle \langle E | 2 \rangle e^{-iEt} \quad (\text{D8})$$

In the presence of hardcore constraint, we have shown that  $\langle E | 2 \rangle \propto \sqrt{k}/\log k$  near the band edge, and  $\rho(E) \propto 1/k$  for the  $l = 0$  sector. In addition,

$$\langle \mathbf{r} | E \rangle = 2C_0(k) \left[ J_0(kr) - \tan \delta_0(k) Y_0(kr) \right]. \quad (\text{D9})$$

where  $C_0(k) = \sqrt{k/2R}$  and  $\tan \delta_0(k) = \mathcal{O}(\frac{1}{\ln k})$  as  $k \rightarrow 0$ . In the energy integral at late times, change of variable implies the dominant momenta scale as  $k \propto 1/\sqrt{t}$ , while the typical separations satisfy  $r \propto \sqrt{t}$  in the noninteracting case, so that  $J_0(kr)$  and  $Y_0(kr)$  remain  $\mathcal{O}(1)$  functions. We therefore make the approximation:

$$\langle \mathbf{r} | E \rangle \approx 2C_0(k) J_0(kr) \left[ 1 + i\mathcal{O}\left(\frac{1}{\log k}\right) \right] \quad (\text{D10})$$

where the imaginary correction  $i\mathcal{O}(\frac{1}{\log k})$  arises because  $J_0(x)$  and  $Y_0(x)$  have an approximate  $\pi/2$  phase difference if  $x$  is not small. Compared with the  $l = 0$  sector in the non-interacting case where  $\langle \mathbf{r} | E \rangle = 2C_0(k) J_0(kr)$  and  $\langle E | 2 \rangle \approx 2C_0(k) \propto \sqrt{k}$ , we can relate the free propagator  $K_0(\mathbf{r}, t)$  to the propagator with hardcore constraint  $K_{hc}(\mathbf{r}, t)$  as

$$K_{hc}(\mathbf{r}, t) = \frac{A}{\log t} K_0(\mathbf{r}, t) \left[ 1 + i\mathcal{O}\left(\frac{1}{\log t}\right) \right] \quad (\text{D11})$$

$$\approx \frac{mA}{\pi i t \ln t} \exp \left[ i \frac{m|\mathbf{r}|^2}{2t} + i\mathcal{O}\left(\frac{1}{\log t}\right) \right] \quad (\text{D12})$$

where  $A$  is a constant. The interaction therefore primarily modifies the propagator amplitude by a logarithmic factor, as expected. However, the planon's typical width is determined by the oscillatory phase, which picks up only an overall phase shift that does not affect the relevant scale  $m|\mathbf{r}|^2/2t$ . Following a similar derivation to Eqs. (D5) and (D6), we therefore conclude that the planon typical width still scales as  $\Delta x_{\perp} \propto \sqrt{h_z t_2}$  in the presence of the hardcore constraint.

## Appendix E: Lineon excitation by the pump pulse

We examine perturbing the system with a time-dependent magnetic field to excite a distribution of lineons pairs. Consider subjecting the system to a pulse of the form

$$V(t) = B(t) \sum_e X_e \quad (\text{E1})$$

where the field  $B(t)$  assumes the form of a Gaussian wave packet of width  $\tau$  and frequency  $\omega$ :

$$B(t) = B_0 \exp\left(-\frac{t^2}{2\tau^2}\right) \cos \omega t \quad (\text{E2})$$

$$= \frac{1}{2} B_0 \exp\left(-\frac{t^2}{2\tau^2}\right) e^{i\omega t} + \text{c.c.} \quad (\text{E3})$$

We parametrize the frequency  $\omega$  as  $\omega = 2\Delta_l + \delta$ , i.e., with detuning  $\delta$  relative to the energy  $2\Delta_l$  to create an isolated pair of lineons. The width  $\tau$  is chosen such that the wave packet contains many oscillations,  $\omega\tau \gg 1$ . In the following, we study the lineon distribution as a function of the parameters entering Eq. (E3).

The state of the system at time  $t$  is given within first-order time-dependent perturbation theory by

$$\langle m | \psi_I(t) \rangle = -i \int_{-\infty}^t ds e^{i(E_m - E_n)s} B(s) \sum_e (X_e)_{mn} \quad (\text{E4})$$

where  $(O)_{mn} \equiv \langle m | O | n \rangle$ . We then make use of the integral

$$\int_{-\infty}^t ds e^{i\omega s - s^2/2\tau^2} = \int_{-\infty}^t ds e^{-(s - i\omega\tau^2)^2/2\tau^2 - \omega^2\tau^2/2} \approx \sqrt{2\pi\tau} e^{-\omega^2\tau^2/2} \quad (\text{E5})$$

where the approximation holds for  $t \gg \tau$ , which allows us to extend the upper limit of integration to infinity. Performing the integral in Eq. (E4) and considering an eigenstate with two lineons along the  $z$ -oriented line at position  $(x, y)$

$$\begin{aligned} \langle x, y; K_z, k_z | \psi_I(t) \rangle \approx & -iB_0\tau \sqrt{\frac{\pi}{2}} \left[ e^{-(E_{mn} + \omega)^2\tau^2/2} + e^{-(E_{mn} - \omega)^2\tau^2/2} \right] \\ & \times \sum_e \bar{A}(K_z, k_z) e^{-iK_z R_e} \sin k_z \quad (\text{E6}) \end{aligned}$$

where  $E_{mn} = E_m - E_n$ . The translation-invariant sum over edges implies that only lineon states with zero center of mass quasimomentum ( $K_z = 0$ ) are excited. For such states,

$$\begin{aligned} \langle x, y; 0, k_z | \psi_I(t) \rangle \approx & -iB_0\tau \sqrt{2\pi} \left[ e^{-(E_{mn} + \omega)^2\tau^2/2} + e^{-(E_{mn} - \omega)^2\tau^2/2} \right] \sin k_z \quad (\text{E7}) \end{aligned}$$

Finally, we neglect the term that is not resonant. Since  $E_m - E_n + \omega \approx 2\omega$ , and we have assumed that  $\omega\tau \gg 1$ , this term is suppressed as  $e^{-2(\omega\tau)^2} \ll 1$ . This leaves us with

$$\langle x, y; 0, k_z | \psi_I(t) \rangle \approx -iB_0\tau\sqrt{2\pi}e^{-[\varepsilon_l(k_z) - \delta]^2\tau^2/2} \sin k_z \quad (\text{E8})$$

where  $\varepsilon_l$  is the energy relative to the bottom of the band. We assume both  $\delta$  and  $\tau^{-1}$  are small compared to the lineon bandwidth (i.e.,  $h_x \gg \delta, \tau^{-1}$ ), so it is appropriate to expand the lineon pair energy  $\varepsilon_l(k)$  near the bottom of the band, giving  $\varepsilon_l(k) = 2h_x k^2 + O(k^4)$ . In the following, we discuss the two parameter regimes  $\delta\tau \gg 1$  and  $\delta\tau \ll 1$  separately.

Lineon excitations affect the braiding probability in two ways: through the lineon velocity and through the lineon excitation density. In the main text, we assume that the lineon pair moves with a characteristic speed  $|v|$ , but in general the excited lineons have a velocity distribution  $p(v)$ , and the braiding probability is modified to

$$P[\mathbf{r}_{1,2}(t); v] \propto \int dv p(v) A[\mathbf{r}_{1,2}(t); v]. \quad (\text{E9})$$

The distribution  $p(v)$  modifies the overall pump-probe coefficient but does not affect the long-time scaling with  $t_2$ . For  $\delta\tau \gg 1$ , the excitations are concentrated on the resonant shell  $\varepsilon_l(k_*) = \delta$  with  $k_* = \sqrt{\delta/(2h_x)}$ . The characteristic velocity is then

$$v(k_*) = \left. \frac{\partial \varepsilon}{\partial k} \right|_{k_*} = 2\sqrt{2h_x\delta}, \quad (\text{E10})$$

which is set by the detuning  $\sqrt{\delta}$ . The width of the distribution  $p(v)$  is controlled by the pulse duration and is of order  $\tau^{-1}$ , and in this regime it is typically smaller than  $v(k_*)$ . In the opposite limit  $\delta\tau \ll 1$ , there is no sharply defined resonant shell, and all states with  $\varepsilon_l(k)\tau \lesssim 1$  have appreciable excitation weight. This leads to a characteristic width of  $p(v)$  that scales as  $\tau^{-1/2}$ . Explicitly, the characteristic momentum is set by  $k_* \approx 1/\sqrt{2h_x\tau}$  and the characteristic velocity becomes

$$v(k_*) \approx 2\sqrt{2h_x/\tau}. \quad (\text{E11})$$

The braiding probability is proportional to the lineon density as long as the excitation density remains sufficiently low. Near the band edge, the lineon density of states exhibits a van Hove singularity (VHS),  $g(\varepsilon_l) \propto 1/\sqrt{\varepsilon_l}$ , since only the mode with quasimomentum  $K_z = 0$  is excited. However, the matrix element vanishes at the band edges as  $|c_k|^2 \propto (\sin k)^2 \sim k^2 \sim \varepsilon_l$ . The lineon density can be evaluated as  $\rho = \int \frac{dk}{2\pi} |c_k|^2 = \int d\varepsilon g(\varepsilon) |c_k|^2$  in two regimes. For  $\delta\tau \ll 1$ ,

$$\rho = \frac{B_0^2}{4h_x} \Gamma(3/4) \tau^{1/2} \left[ 1 + 2 \frac{\Gamma(5/4)}{\Gamma(3/4)} (\delta\tau) + O(\delta^2\tau^2) \right] \quad (\text{E12})$$

Therefore, the expected VHS at the band edge is regularized in linear response. For  $\delta\tau \gg 1$ ,

$$\rho = \frac{\sqrt{\pi}B_0^2}{2h_x} \tau \delta^{1/2} [1 + O((\tau\delta)^{-2})]. \quad (\text{E13})$$

Combining the results for the lineon density with the characteristic velocity and keeping only the leading order, we obtain (at a fixed time  $t_2$ ):

$$\chi_{pp}(\tau, \delta) \propto \begin{cases} \chi^{(1)} \times \tau^0 \delta^0, & \delta\tau \ll 1 \\ \chi^{(1)} \times \tau \delta, & \delta\tau \gg 1 \end{cases} \quad (\text{E14})$$

where  $\chi^{(1)}$  is the linear-response susceptibility of the planons created by the probe pulse, while  $\tau$  and  $\delta$  are pump parameters that control the excitation of lineons. Although the VHS in the lineon's DOS does not show up,  $\chi^{(1)}$  might have a VHS at half filling due to the effective 2D tight-binding Hamiltonian of planons.

## Appendix F: Tuning static magnetic field

So far, we have assumed that both  $h_x$  and  $h_z$  in the static magnetic field are finite, so that both lineons and planons acquire dynamics. Since the excitation energies of a lineon pair and a planon pair depend on  $h_x$  and  $h_z$ , respectively, a small change in the direction of the static field  $\mathbf{h}$  effectively tunes the resonance frequencies of the pump and probe pulses. In addition, we can study some extreme cases of  $\mathbf{h}$ . In the limit  $h_x \rightarrow 0$ , the lineon pair is immobile and does not spread. Consequently, the planons can braid either zero or two lineons, both of which yield a trivial statistical phase; hence the braiding-induced nonlinear response vanishes. In contrast, because the lineons remain spatially localized, the linear response associated with lineon excitations is expected to be enhanced and longer-lived (non-decaying). Turning on a small but finite  $h_x$  while keeping  $h_z/h_x \gg 1$ , the pump-probe signal may exhibit distinct scaling at a finite time window. Recall that for planon extended states, the parallel width scales as  $\Delta x_{\parallel} \sim |v|t_2 + O(\sqrt{h_z t_2})$  where the subleading term arises from the quantum spreading of the planon pair along the direction parallel to the lineon velocity. This implies a crossover for the two contributions at a critical time  $t_c$  when  $|v|t_c \sim \sqrt{h_z t_c}$ . For  $t_2 \gg t_c$ , the lineon velocity contribution dominates, and we expect the usual scaling  $\chi_{pp} \propto \sqrt{t_2}/\log(t_2)^2$ . In contrast, for  $t_2 \ll t_c$ , the planon's spreading term dominates so that  $\Delta x_{\parallel} \sim \sqrt{h_z t_c}$ , correspondingly the pump-probe signal decreases with time as  $\chi_{pp} \propto 1/\log(t_2)^2$ . Since the lineon velocity scales as  $|v| \propto \sqrt{h_x}$ , the critical time scales as  $t_c \propto \sqrt{h_z/h_x}$ . Therefore, in the regime  $h_z/h_x \gg 1$  (with finite  $h_x$  and a long delay time  $t_1$ , so that the lineon pair is far separated), there exists a broad time window  $\Delta t \propto \sqrt{h_z/h_x}$  during which the nonlinear response is decreasing. Note that this argument does not apply to the planon bound state, for

which  $\Delta x_{\parallel} \sim |v|t_2$  always. In the opposite limit  $h_z \rightarrow 0$ , planons become immobile, so the planon's linear response is enhanced and long-lived. For the braiding contribution,  $\Delta x_{\perp} \sim 1$  and  $\Delta x_{\parallel} \propto |v|t_2$ , therefore, the pump-probe

signal  $\chi_{pp} \propto t_2$ . To conclude, tuning the direction of the static magnetic field provides different signatures of the linear and nonlinear response.

- 
- [1] R. M. Nandkishore and M. Hermele, Fractons, *Annual Review of Condensed Matter Physics* **10**, 295 (2019).
  - [2] M. Pretko, X. Chen, and Y. You, Fracton phases of matter, *International Journal of Modern Physics A* **35**, 2030003 (2020).
  - [3] A. Gromov and L. Radzihovsky, Colloquium: fracton matter, *Reviews of Modern Physics* **96**, 011001 (2024).
  - [4] R. M. Nandkishore, W. Choi, and Y. B. Kim, Spectroscopic fingerprints of gapped quantum spin liquids, both conventional and fractonic, *Phys. Rev. Res.* **3**, 013254 (2021).
  - [5] S. Mukamel, Principles of nonlinear optical spectroscopy, (No Title) (1995).
  - [6] M. McGinley, M. Fava, and S. A. Parameswaran, Signatures of fractional statistics in nonlinear pump-probe spectroscopy, *Phys. Rev. Lett.* **132**, 066702 (2024).
  - [7] X. Yang, R. Buechele, and N. Trivedi, Detection of anyon braiding through pump-probe spectroscopy (2025), [arXiv:2503.22792](https://arxiv.org/abs/2503.22792) [cond-mat.str-el].
  - [8] N. Kirchner, W. Choi, and F. Pollmann, Measuring anyonic exchange phases using two-dimensional coherent spectroscopy (2025), [arXiv:2511.17420](https://arxiv.org/abs/2511.17420) [cond-mat.str-el].
  - [9] S. Pai and M. Hermele, Fracton fusion and statistics, *Phys. Rev. B* **100**, 195136 (2019).
  - [10] S. Vijay, J. Haah, and L. Fu, Fracton topological order, generalized lattice gauge theory, and duality, *Phys. Rev. B* **94**, 235157 (2016).
  - [11] C. Castelnovo, C. Chamon, and D. Sherrington, Quantum mechanical and information theoretic view on classical glass transitions, *Phys. Rev. B* **81**, 184303 (2010).